The University of Reading

School of Mathematical and Physical Sciences

Heat Transfer in a Buried Pipe

Martin Conway

August 2010

This dissertation is a joint MSc in the Departments of Mathematics & Meteorology and is submitted in partial fulfilment of the requirements for the degree of Master of Science

DECLARATION:

I con rm that this is my own work, and the use of all material from other sources has been properly and fully acknowledged.

Signed .....

ACKNOWLEDGEMENTS:

I would like to thank my supervisors Dr. Stepher Langdon and Prof. Mike Baines for their help and advice during the course of this dissertation. I would also like to thank the NERC for their nancial support.

Abstract

In this dissertation, we are considering the heat transfer from a pipe buried underground. This is a classic heat di usion problem which has many applications in the oil and gas industry as well as other agricultural and domestic uses. The simpli ed problem under consideration in this dissertation concerns an underground pipe with circular cross-section buried in soil which we assume has constant thermal properties. Heat di uses with a given ux rate across the boundary of the pipe, and at a di erent ux rate at ground level. We are interested in the temperature distribution below the ground surface, exterior to the pipe when the temperature is in a steady state. Since there is no time dependency, we are e ectively solving Laplace's Equation in two dimensions on an exterior domain with Neumann boundary conditions given on the pipe boundary and at the ground surface.

The aim of this dissertation is to derive an accurate numerical solution using Boundary Element Methods. There are several methods we could deploy to solve this equation, depending on the boundary conditions, but we will demonstrate why this method is highly suitable for this particular problem. There will be numerous examples given to demonstrate that an accurate solution has been achieved and we will also highlight techniques which enhance accuracy often for very little extra computational cost. The examples given may not necessarily accurately re ect real world physical situations - rather the aim is to be able to benchmark numerical solutions versus analytic solutions where possible so that we can prove the method to be robust.

Contents

1 Introduction

1.1 Background

The problem of heat transfer from a buried pipe is a classic heat conduction problem that has many applications in the real world. These applications can be as small-scale as under oor heating systems such as the Ondol system used in Korea which uses heat generated from cooking stoves [7], to more large scale applications such as oil or gas pipelines either under the seabed or underground. Agriculture has other applications for the consideration of heat transfer of pipes [8]. Soil warming in agriculture is an e cient method of increasing crop yield and growth rates, and can be cost-e ective if it uses low energy sources such as industrial waste heat, geothermal or solar energy.

The oil industry clearly has a major interest in the eld of heat transfer from buried pipes, and many research companies [13] devote considerable resources trying to model the e ects for the large oil and gas companies. One reason for this is that temperature and pressure a ect the viscosity of the uid travelling through the pipeline. This can, in turn, determine the state of the uid owing through the pipe (i.e. liquid or gas). Another concern particularly with increasing volumes of oil and gas coming from Arctic regions is the e ect of freezing around oil and gas pipes in the vicinity of permafrost [15]. Of importance here is the outward advance of the thaw front around the warm pipe.

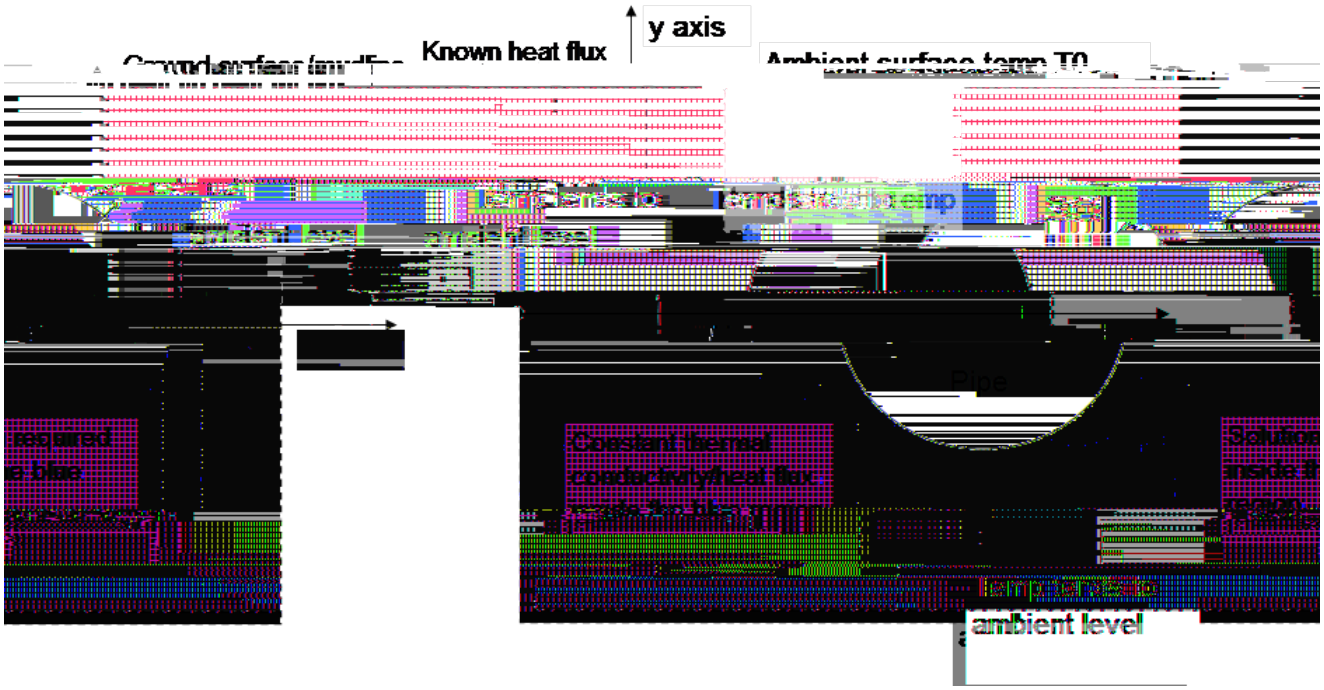

Figure 1: Schematic of the physical situation

1.2 Governing equation

The starting point for our model is derived from Fourier's Law [21] which speci es that heat transfer is governed by the equation:

$$q = \quad r u \tag{1}$$

where:

q heat ux vector per unit length

heat conductivity of the soil

u temperature throughout the region.

If our system is in steady-state, then Conservation of Energy [21] implies that, in the absence of heat sinks or sources, the heat ux throughout the region must satisfy:

$$r \quad q = 0: \tag{2}$$

In one dimension, this would imply that heat ux must be constant at all points; in more than one dimension, it implies that heat ux entering a control region must equal heat ux leaving the same region. If we assume that all thermal properties are constant, then is constant and (2) reduces to Laplace's Equation:

$$r^2 u = 0:$$

surface due to lack of sunlight and moisture considerations. However, in some deep mines (4 km underground) in South Africa for example, temperatures have been known to climb to around 55 *C*, well

where we have used the fact that u_n must not blow up as $r \to \infty$ and u_n is 2π-periodic. Furthermore,

$$
\begin{aligned}
A_n &= \frac{a^2}{\pi} \int_0^{2\pi} f(\theta) \cos n\theta \, d\theta \\
B_n &= \frac{a^2}{\pi} \int_0^{2\pi} f(\theta) \sin n\theta \, d\theta \, . \qquad (6)
\end{aligned}
$$

Thus for a simple closed-form solution, we could for example choose f to be $\sin\theta$ or $\cos\theta$ which would leave u with one term only. A solution as an infinite sum could be reduced down to a simpler integral form but this would still require numerical methods to solve and would not be that useful as a benchmark.

The second scenario where we may be able to obtain an analytic solution is when the pipe is exactly half-buried. In this case, our boundary conditions apply along the constant lines $r = a; \ \theta = \pi; \ \theta = 2\pi$. Our ability to produce a simple analytical expression depends on the boundary conditions. For example, using the following boundary conditions:

$$
\begin{aligned}
f(\theta) &= \sin 2\theta \\
g(x) &= \frac{a^3}{x^3}
\end{aligned}
$$

would yield the closed-form solution, $u = \dfrac{a^3 \sin 2\theta}{2r^2}$, where a is the radius of the pipe. Again, this solution would provide useful benchmarking for our numerical solution.

1.4.2 Finite Difference and Finite Element Methods

The finite diererence (FD) method is often used as a brute force method to solve many Partial Differential Equations (PDEs) as it is often easy to set up and understand [9, pp. 167{187]. A two dimensional regular mesh ($N \times M$ grid points) is constructed on the region in which we are looking for a solution, using Cartesian coordinates in this case. At each mesh point $(x_i; y_j)$, we use the discretised version of Laplace's Equation:

$(u_i$2i), we use the discretised version of Laplace's

Tf 4.198 1.494 Td [(),)-290(w)28(e)-280(use)-279(the)-280(di)1Laplace's

Although the matrix above would be sparse (many of the elements would be zero), storing such large data structures could have an adverse e ect on computational speeds.

Hence for problem (3), we do not expect the Finite Di erence Method to provide an acceptably quick and accurate solution.

1.4.3 Conformal mapping

This technique maps the physical region onto a rectangular domain by using a complex transformation [7]:

$$w = \ln \left(\frac{z - ip\sqrt{h^2 - a^2}}{z + ip\sqrt{h^2 - a^2}} \right) :$$

The transformed boundaries now form the boundary of a rectangle in the complex domain which may be easier to handle using separation of variables, although the boundary conditions are di erent and may be more di cult to handle. For most problems, however, numerical methods may still be involved so this does not necessarily help us solve the problem.

For a much more detailed discussion, refer to [7].

1.4.4 Bipolar coordinates

There are two standard de nitions for bipolar coordinate systems:

Bipolar coordinates (;). These are de ned in Wikipedia [18] as follows:

$$\begin{aligned} x &= a\frac{\sinh}{\cosh \quad \cos} \\ y &= a\frac{\sin}{\cosh \quad \cos} \end{aligned} \tag{7}$$

where the -coordinate of a point P equals the angle F_1PF_2 and the -coordinate is given by $= \ln \frac{d_1}{d_2}$, where $d_1; d_2$ are the distances to the two foci $F_1; F_2$ located at ($a;0$) and ($+a;0$) respectively, as shown in Figure 2.

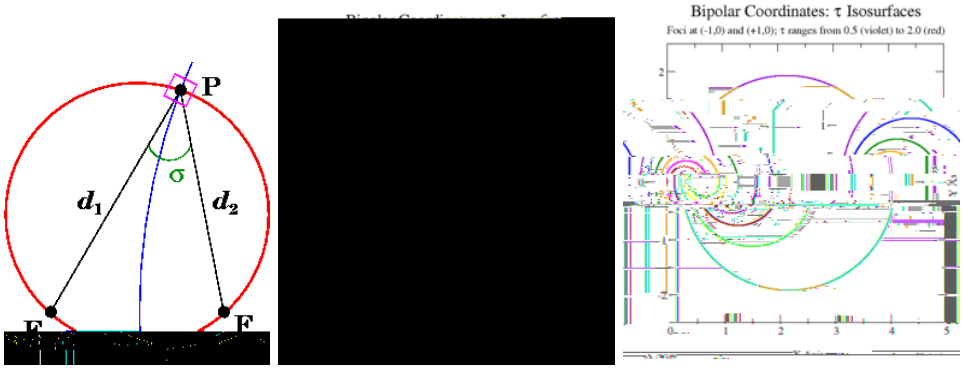

Figure 2: Illustration of bipolar coordinates ; [18]

In (;) coordinates, $r^2 = \frac{1}{a^2}(\cosh \quad \cosh \ )^2(\frac{@^2}{@ \ ^2} + \frac{@^2}{@ \ ^2})$.

Two-centre bipolar coordinates $(r_1; r_2)$ [20]. For a given point $\mathbf{p} = (x; y)$, then r_1 is the distance between $\mathbf{p}$ and the point $(\ a; 0)$ and r_2 is the distance between $\mathbf{p}$ and the point $(+a; 0)$.

$$r_1 = \sqrt{(x + a)^2 + y^2}$$
$$r_2 = \sqrt{(x \ \ a)^2 + y^2}:$$

Simple rearrangement yields the transformation to Cartesian coordinates from bipolars $(r_1; r_2)$:

$$x = \frac{r_1^2 \ \ r_2^2}{4a}$$
$$y = \frac{1}{4a}\sqrt{16a^2 r_1^2 \ \ (r_1^2 \ \ r_2^2 + 4a^2)^2}: \qquad (8)$$

Whilst either of these coordinate systems may be of use solving problem (3), we have not focussed on this method of solution in this dissertation. Elsewhere, analytic solutions have been obtained through this method (see [13],[14]).

1.4.5 Boundary Element Methods

This approach works when the PDE we are looking to solve has a simple Fundamental Solution associated with it. In the case of Laplace's Equation, the Fundamental Solution at a point $\mathbf{p} = (x_p; y_p)$ [illegible]

2 Formulating the Boundary Integral Equation

2.1 Background

Given the complicated nature of the di erent domains and boundaries we need to consider, it is helpful to de ne these in detail for later reference (see Figure 3).

Let the origin of our Cartesian $(x; y)$ plane, O, be at the centre of the oil pipe.

Let D_a be the interior of circular pipe radius a, with boundary $_a$.

Let the large bounded domain D_{box} be de ned by the interior of the region enclosed by the lines $y = Y; x = R; y = R; x = +R$.

Let the boundary of D_{box} be $_1; _2; _3; _4$ as shown in.9626 Tf 7.642 ;iaralm9626 Tetw wher

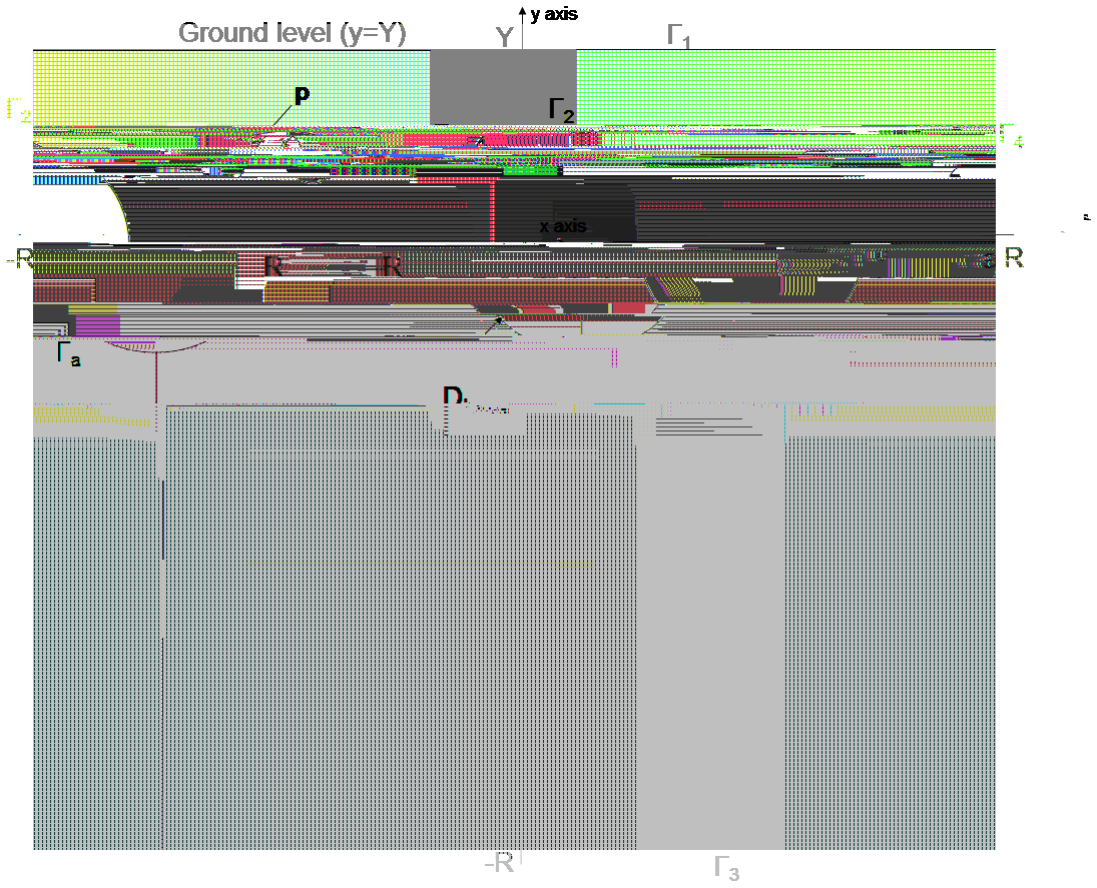

Figure 3: Layout of the di erent domains and boundaries

To formulate our BIE and to specify constraints on our boundary conditions, we will also need to regularly make use of Green's Second Identity [11, p.69] . This states that if and are twice continuously di erentiable on D in R^2 then:

$$\iint_D (\quad r^2$$

so that $v \to 0$ as $|x|, |y| \to \infty$. v is still harmonic on D and $\frac{\partial v}{\partial n} = \frac{\partial u}{\partial n} - c n_y$ where n_y is the y component of the outward normal vector to the boundary.

In order that the solution v does not blow up as $|R| \to \infty$, we need to stipulate that for some real > 0:

$$\begin{aligned} \frac{\partial v}{\partial x} &= O(|x|^{-(1+\alpha)}) \text{ as } |x| \to \infty \\ \frac{\partial v}{\partial y} &= O(|y|^{-(1+\alpha)}) \text{ as } y \to -\infty \end{aligned} \tag{12}$$

$v \to 0$ as $|x|, |y| \to \infty$; (which immediately follows from our first assumption).

We will see later in §2.4 that this together with compatability (see below) is sufficient to guarantee existence of a unique solution to (3).

For any harmonic function v in D, substituting $= v$ and $= 1$ into (10), we get:

$$\int_{\Gamma} \frac{\partial v}{\partial n} ds = 0. \tag{13}$$

Rewriting boundary conditions for v as $\tilde{f} = f + c \sin$ on Γ_a and $\tilde{g} = g - c$ on Γ_1, then as $R \to \infty$ the integrals over $\Gamma_2, \Gamma_3, \Gamma_4$ disappear and the above condition (13) reduces to:

$$\int_{\Gamma_a} \tilde{f} ds + \int_{\Gamma_1} \tilde{g} ds = 0. \tag{14}$$

This is known as the **compatability condition**.

Since $f = \tilde{f} - c \sin$ and $g = \tilde{g} + c$, it follows that we require:

$$\int_{\Gamma_a} f ds + \int_{\Gamma_1} g ds = 0$$

as all integrals involving the constant c sum to 0.

2.3 Formulation of BIE

To formulate our BIE using the Direct Method, we could make use of (10) by substituting $= v$ and $= G$. 8 9.9626 Tf 8.463 0 T5]TJ/F9 4.9x(0409.9626 Tf 10.516 0 d [15)]TJ/F11 ar8(v)27(harmonic333(in)is)-333D,3(it

$Z_{g/F8\ 9.962.833\ 0\ Td\ [(.)-444=}$

function G using method of images such that $\frac{@G}{@n} = 0$ on $_1$.

The modi ed Green's function G is de ned by:

$$G(x_p; y_p j x_q; y_q) = G(x_p; y_p j x_q; y_q) + G(x_p; y_p j x_q; y_{q'}), \text{ where } y_{q'} = 2Y \quad y_q: \tag{16}$$

On $_1$:

$$\frac{@G}{@n} = \frac{@G}{@y_q} = \frac{@G(x_p; y_p j x_q; y_q)}{@y_q}_{y_q = Y} \quad \frac{@G(x_p; y_p j x_q; y_{q'})}{@y_{q'}}_{y_{q'} = Y} = 0: \tag{17}$$

G now has two singularities both of which are outside the domain D. Therefore within D, G is still harmonic and so we can still use Green's Second Identity to formulate our BIE.

Using our modi ed Green's function we can now state that for p 2 D:

$$Z \quad v(q)\frac{@G(p; q)}{@n_q} \quad G(p; q)\frac{@v(q)}{@n_q}\Bigg! \, ds_q = 0: \tag{18}$$

which will only incorporate values of v on $_a$ and since $\frac{@G}{@n} = 0$ on $_1$. We set out below each element of the above integral and will prove each result in turn.

2.4 Theorems

Theorem 1. *If* p 2 D *and* q 2 $_a$, *and* G *is as de ned in* (16), *then for any* $f \in C; v$ *satis es:*

$$Z \quad \Big" v(q)\frac{@G(p; q)}{@n_q} \quad G(p; q)\frac{@v(q)}{@n_q}\Big\# ds_q = a \int_0^{Z\ 2} \Big" v( ) \quad \frac{@G(p; q)}{@x_q}\cos \ + \frac{@G(p; q)}{@y_q}\sin \ \Big! + G(p; q)f( ) \Big\# d \tag{19}$$

where q $= (x_q; y_q) = (a\cos \ ; a\sin \ )$.

Furthermore, if p 2 $_a$,

$$Z \quad \Big" v(q)\frac{@G}{@n_q}(p \ ; q) \quad G(p \ ; q)\frac{@v}{@n_q}(q) \Big\# ds_q = \int_{\#^0}^{Z\ 2} v( ) \ \frac{1}{4} + a\frac{@G}{@x_q}(p^{'}; q)\cos \ + a\frac{@G}{@y_q}(p^{'}; q)\sin \ d$$

q) *ds*

Since $_a$ describes a circle, $\mathbf{n_q} = (\cos ; \sin)$. Therefore $\frac{\partial G}{\partial n_q} = \frac{\partial G}{\partial x_q} \cos \quad \frac{\partial G}{\partial y_q} \sin$.
In this case, ds_q describes small changes in arc length, therefore $ds_q = ad$.
Finally we can substitute $\frac{\partial v}{\partial n_q} = \tilde{f}$ on $_a$, leading to equation (19).

To prove equation (20), rst observe that for $p \in {}_a$:

$$\frac{\partial G}{\partial x_q}(p ; q) = \frac{(x_q \quad x_p)}{2 \quad [(x_q \quad x_p)^2 + (y_q \quad y_p)^2]}$$

$$\frac{\partial G}{\partial y_q}(p ; q) = \frac{(y_q \quad y_p)}{2 \quad [(x_q \quad x_p)^2 + (y_q \quad y_p)^2]}$$

2 Wt4.885t 3TJ/F8 90Tf 6 's 8TJ/Ffunct973.962209.31 558.987(K1J/F603363.8.3Tf 69]TJ/F8 9.9[(y)]TJ/F10 6.9738 Tf .319 9.962 0501

and substitute in the trigonometric exp.96-30.526 Td [(an(C4)-333(subs1.494 Td [(Gnasf 0 Td [(Td [(@)-56(y)] 1 9945.

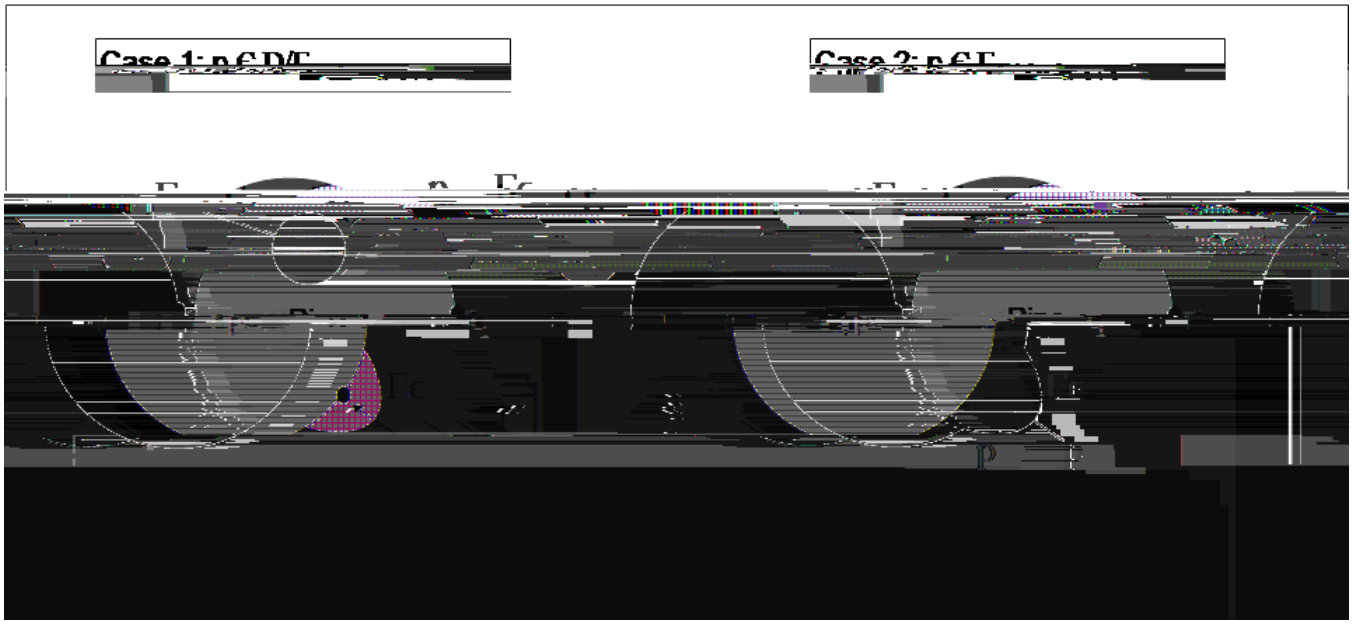

Figure 4: Showing load point p in D, and on $_a$

It follows immediately that:

lim
$_!$

Also since $v \to 0$ as $|x| \to 1$, there exists $x_1 \in \mathbb{R}$ such that for any $\varepsilon > 0$, $|v| < \varepsilon$ for all $x > x_1$. Therefore for $R > \max(x_0, x_1)$ we can rewrite LHS of (35) as:

$$\begin{aligned}
&\int_R^R \left(v\frac{\partial G}{\partial x_q}\right)_{x_q = R} - \left(G\frac{\partial v}{\partial x_q}\right)_{x_q = R} dy_q \\
&\quad = \int_R^R v(R; y_q)\frac{\partial G}{\partial x_q}(x_p; y_p | R; y_q)\, dy_q + \int_R^R G(x_p; y_p | R; y_q)\frac{\partial v}{\partial x_q}(R; y_q)\, dy_q \\
&\quad \le \int_R^R \frac{\partial G}{\partial x_q}(x_p; y_p | R; y_q)\, dy_q + MR^{-(1+\varepsilon)} \int_R^R G(x_p; y_p | R; y_q)\, dy_q \\
&\quad = \frac{1}{2\pi}\int_R^R \frac{(R - x_p)}{(R - x_p)^2 + (y_p - y_q)^2}\, dy_q \\
&\qquad + \frac{MR^{-(1+\varepsilon)}}{4\pi}\int_R^R \ln[(R - x_p)^2 + (y_q - y_p)^2]\, dy_q \\
&\quad \le \frac{1}{2\pi}\frac{2R}{(R - x_p)} + \frac{MR^{-(1+\varepsilon)}}{4\pi} 2R \ln(8R^2) \\
&\quad = \frac{1}{(1 - \frac{x_p}{R})} + \frac{(\ln 8 + 2\ln R)MR^{-\varepsilon}}{2\pi}. \qquad (36)
\end{aligned}$$

As $R \to 1$ and $\varepsilon \to 0$, the i09i9/;term09i9/;clearly09i9/;tendsheTvthelim00

!278;0As

R -4 [(R)]TJ/0F7 6.9738 T14 5.192 3.8 0 Td [( )]TJ/F8 9.9626 T9 7.193.95642 Td [(!278;0.)1

same operators (referencing any point in the domain) using those boundary values to solve the equation for that point in the domain.

In this example, we have the following operator representation:

$$v(\mathrm{p}) \quad (Av)(\mathrm{p}) = (Bf)(\mathrm{p}) + (Cg)(\mathrm{p}) \text{ for } \mathrm{p} \in D \tag{38}$$

$$\frac{v(\mathrm{p})}{2} \quad (Av)(\mathrm{p}) = (Bf)(\mathrm{p}) + (Cg)(\mathrm{p}) \text{ for } \mathrm{p} \in a \tag{39}$$

where:

$$Az(\mathrm{p}) = \int_a z(\mathrm{q}) \frac{\partial G}{\partial n_q}(\mathrm{p};\mathrm{q})\, ds_q$$

$$Bz(\mathrm{p}) = \int_a G(\mathrm{p};\mathrm{q}) z(\mathrm{q})\, ds_q$$

$$Cz(\mathrm{p}) = \int_1 G(\mathrm{p};\mathrm{q}) z(\mathrm{q})\, ds_q.$$

3 Numerical Methods for solving Boundary Integral Equations

3.1 Background

In the previous section, we formulated the BIE which we need to solve on $_a$. In general, this equation cannot be solved analytically, so we need to develop some numerical techniques to provide the solution. The goal here is to approximate the continuous operators using discrete operators on v so that a linear system of equations on v can then be solved using matrix inversion.

There are several techniques for discretising the BIE; the ones we will look at in this dissertation are known as Nystrom's Method and the Collocation Method. Although Galerkin's Method is popular amongst mathematicians due to some of its elegant analytical properties, we will not be discussing it further.

Accuracy in our numerical integration techniques is also critical as this will allow us to use fewer sample points and hence decrease calculation times. Therefore we will be examining di erent numerical integration rules (known as quadrature), namely the trapezium rule and Gauss-Legendre quadrature, with a view to how precision can be optimised whilst not impacting calculation speeds too adversely.

Finally we will look at some simple examples where the analytic solution is known so we can compare accuracy for the various methods and present some numerical results. This will include examples where the pipe is buried deep underground, and a sequence of results as the pipe approaches ground level.

3.2 Quadrature

Throughout the following discussion, there are numerous references to the term quadrature and the rules used to perform numerical integration. Therefore it would be helpful to set out some de nitions here to make the subsequent material clearer.

3.2.1 De nition

A quadrature rule is a numerical approximation for a de nite integral, $I = \int_a^b f(x)dx$. In general, an N-point quadrature rule would approximate the integral as:

$$I \quad \sum_{i=1}^{N} w_i f(x_i)$$

where w_i are called the weights and x_i are called the abscissas.
As a simple example, the trapezium rule would approximate the integral as follows:

$$I \quad \frac{(b \quad a)}{2}(f(a) + f(b))$$

and would therefore be termed a 2-point quadrature rule. Here we have speci ed the abscissas $x_1 = a; x_2 = b$ and solved for the weights $w_1; w_2$ to ensure that I is exact when f is any polynomial of order 1 since this gives us two equations in two unknowns.

If the range of integration is subdivided into N equal partitions $[x_i; x_{i+1}]$ where $i = 1;:::;N$, we get the composite version of the trapezium rule:

$$\sum_{n=1}^{N}$$

The weights are then de ned as:

$$w_i = \frac{2(1 \quad x_i^2)}{N^2[P_N \quad 1.8 \text{ ff} 6.(\quad 8 \text{ ff} 6.396 \quad 6.72.879 \text{ d}[()]\text{TJETE3 } 5626 \text{ ff} 9.962 \text{ 0 d}[()]\text{TJETE7 } 6.9738 \text{ ff} 7.132 \text{ -1.494 d}[()]\text{TJETE3.3 ff}}$$

This suggests that the optimal value for in this scenario would be around 0.20. In practice, when more weights are used an optimal of 0.15 is commonly used [12], and this is the value we have used in our examples later on. As a further comparison, when we use 16 weights with no grading, $I = 2.170295$ which gives an error of 0.335%.

3.3 Discretisation Methods

3.3.1 Nystrom's Method

Perhaps the simplest discretisation method to understand is Nystrom's Method [2, pp. 100{103] which gives a quick and e cient way to discretise BIEs of the Second Kind, using the quadrature rule of our choice to approximate the integral.

In general, suppose we have a BIE such as:

$$v(\mathbf{p}) \quad Av(\mathbf{p}) = h(\mathbf{p})$$

where $A = \int K(\mathbf{p};\mathbf{q})v(\mathbf{q})ds_q$ and K is a continuous kernel.

We can use a quadrature rule on the operator A such that:

$$(Av)(\mathbf{p}) \quad \sum_{j=1}^{N} w_j K(\mathbf{p};\mathbf{q_j})v(\mathbf{q_j})$$

Now suppose that our approximation for v using N node points is v_N, then we can de ne v_N as follows:

$$v_N(\mathbf{p}) \quad \sum_{j=1}^{N} w_j K(\mathbf{p};\mathbf{q_j})v_N(\mathbf{q_j}) = h(\mathbf{p}) \tag{48}$$

At each node point, p_i where $i = 1;:::;N$:

$$v_N(\mathbf{p_i}) \quad \sum_{j=1}^{N} w_j K(\mathbf{p_i};\mathbf{q_j})v_N(\mathbf{q_j}) = h(\mathbf{p_i}) \tag{49}$$

which is a linear system for v_N of order N which can be solved by matrix inversion.

For other points $\mathbf{p} \in D$, we can then write:

$$v_N(\mathbf{p}) = \sum_{j=1}^{N} w_j K(\mathbf{p};\mathbf{q_j})v_N(\mathbf{q_j}) + h(\mathbf{p}) \tag{50}$$

Equation (50) is known as Nystrom's interpolation formula and is the key to maintaining the accuracy of the solution. This method works well when the kernel K is continuous everywhere and does not contain singularities. In the problem we are looking at however, the kernel of the operator A is the derivative of the Green's function which will become singular for any point p approaching the boundary $_a$. In this

3.4 Basis functions

The next step in implementing the numerical method is to choose suitable basis functions that we can use in (51). This often depends on factors such as nature of boundary conditions, accuracy required, ease of implementation, speed of computation. Common basis functions include:

Piecewise constant e.g.

$$_j(x) = \begin{cases} 1 & \text{if } x \ 2 \ X_j \\ 0 & \text{if } x \ \not 2 \ X_j : \end{cases} \tag{54}$$

Alternative de nitions for X_j are $[x_{j\ 1}; x_j]; [x_j; x_{j+1}]$ or for regularly spaced nodes $[x_j \quad \frac{x}{2}; x_j + \frac{x}{2}]$.

Piecewise linear e.g.

$$_j(x) = \begin{cases} \dfrac{x \quad x_{j\ 1}}{x_j \quad x_{j\ 1}} & \text{if } x \ 2 \ [x_{j\ 1}; x_j] \\ \dfrac{x_{j+1} \quad x}{x_{j+1} \quad x_j} & \text{if } x \ 2 \ [x_j; x_{j+1}] \\ 0 & \text{otherwise.} \end{cases} \tag{55}$$

Piecewise polynomial e.g. Lagrange polynomial basis

$$_1^N(x) = \frac{(x \quad x_0)(x \quad x_2)(x \quad x_3)::::(x \quad x_N)}{(x_1 \quad x_0)(x_1 \quad x_2)(x_1 \quad x_3)::::(x_1 \quad x_N)}$$

$$_j^N(x) = \frac{(x \quad x_0)(x \quad x_1)::::(x \quad x_{j\ 1})(x \quad x_{j+1})::::(x \quad x_N)}{(x_j \quad x_0)(x_j \quad x_1)::::(x_j \quad x_{j\ 1})(x_j \quad x_{j+1})::::(x_j \quad x_N)} :$$

Hence $_j^N(x_k) = \ _{jk}:$ (56)

Trigonometric basis e.g. Lagrange basis functions where 2N points are evenly spaced around a circular boundary [11, p. 182]

$$_j^N(x) = \frac{1}{2N} \left\{ 1 + \cos N(x \quad x_j) + 2 \sum_{n=1}^{N\ 1} \cos n \right.$$

Next consider the geometric series:

$$\sum_{n=1}^{N-1} e^{in(x_k - x_j)} = \frac{1 - e^{i(k-j)2\pi}}{1 - e^{\frac{i(k-j)2\pi}{N}}} - 1$$
$$= 1. \tag{58}$$

Therefore, $\frac{1}{2N}\left[1 + \cos N(x_k - x_j) + 2\sum_{n=1}^{N-1} \cos n(x_k - x_j)\right] = 0$ for $j \neq k$.

Hence, $\ell_j^N(x_k) = \delta_{jk}$. □

If we express v in terms of basis functions $\{\ell_j\}_{j=1}^{M}$ as defined in (57) so that $v(\theta) \approx \sum_{j=1}^{M} \ell_j(\theta) v(\theta_j)$ where $M = 2N$ is an even number, then:

$$Av \approx \int_a^{2\pi} \frac{\partial G}{\partial n}(\theta, \tau) \sum_{j=1}^{M} \ell_j(\tau) v(\theta_j) d\tau \tag{59}$$

$$\sum_{j=1}^{M} v(\theta_j) \int_a^{2\pi} \frac{\partial G}{\partial n}(\theta, \tau) \ell_j(\tau) d\tau \tag{60}$$

If we now use the composite trapezium rule as described in (45) to numerically integrate, we get the following expression:

$$Av \approx \sum_{j=1}^{M} v(\theta_j) \frac{\partial G}{\partial n}(\theta, \theta_j) \tag{61}$$

where $= \frac{2\pi}{M}$.

This result shows that if our quadrature rule is the composite trapezium rule, and the collocation points are the same as the sample points, then Nystrom's Method and the Collocation Method are in fact equivalent.

We shall see in the *x*3.7.2 that because $\frac{\partial G}{\partial n}(\theta, \tau)$, $\ell_j(\tau)$ and every derivative of these functions are all 2π-periodic, then the substitution

$$\int_a^{2\pi} \frac{\partial G}{\partial n}(\theta, \tau) \ell_j(\tau) d\tau = \sum_{j=1}^{M} \frac{\partial G}{\partial n}(\theta, \theta_j)$$

has arbitrarily small error for sufficiently large M.

3.5 Singular Kernels

When calculating $B\tilde{f}$, a problem arises since G has a singularity on Γ_a. Therefore if we were simply to apply the composite Trapezium Rule to numerically integrate we may generate significant errors. However, since the singular kernel in this case is logarithmic, we express $\tilde{f}$ in terms of the Lagrangian

trigonometric basis functions $\{L_j\}$, defined below, to resolve this problem. We can then integrate the

Therefore,

$$
\begin{aligned}
2I_0 &= \int_0^{2} \ln\left(4\sin^2\frac{}{2}\right) + \int_0^{2} \ln\left(4\cos^2\frac{}{2}\right) d \\
&= \int_0^{2} \ln\left(16\sin^2\frac{}{2}\cos^2\frac{}{2}\right) d \\
&= \int_0^{2} \ln\left(4\sin^2\right) d \\
&= \frac{1}{2}\int_0^{4} \ln\left(4\sin^2\frac{}{2}\right) d \\
&= I_0.
\end{aligned}
$$

Hence $I_0 = 0$.

For the case where k 1, we need to make use of the geometric sum:

$$
1 + e^{ik} + 2\sum_{j=1}^{k-1} e^{ij} = 1 + e^{ik} + 2
$$

Comparing real and imaginary parts, this yields:

$$\int_0^{2\pi} \cos k\theta \cot\frac{\theta}{2}\,d\theta = 0$$
$$\int_0^{2\pi} \sin k\theta \cot\frac{\theta}{2}\,d\theta = 2\pi : \tag{69}$$

If we integrate the real part of (63) by parts we obtain:

$$\begin{aligned}\int_0^{2\pi} \ln\left|4\sin^2\frac{\theta}{2}\right| \cos k\theta\, d\theta &= \ln\left|4\sin^2\frac{\theta}{2}\right| \frac{\sin k\theta}{k}\Bigg|_0^{2\pi} - \frac{1}{k}\int_0^{2\pi} \frac{4\sin\frac{\theta}{2}\cos\frac{\theta}{2}\sin k\theta}{4\sin^2\frac{\theta}{2}}\,d\theta \\ &= 0 - \frac{1}{k}\int_0^{2\pi} \sin k\theta \cot\frac{\theta}{2}\,d\theta \\ &= -\frac{2\pi}{k}\end{aligned} \tag{70}$$

using the result (69).

Since I_k is real, then it follows that $I_{-k} = I_k$. Hence for integer values of $k \neq 0$, the value of our integral is $\frac{2\pi}{|k|}$, and our proof is complete. □

Substituting this into (62) we now get:

$$\begin{aligned}w_j(\theta) &= \int_0^{2\pi} L_j(\theta+\phi) \ln\left|4a^2\sin^2\frac{\phi}{2}\right| d\phi \\ &= \frac{1}{2N}\int_0^{2\pi} \ln a^2 + \ln\left|4\sin^2\frac{\phi}{2}\right| \left\{1 + \cos N(\theta - \theta_j + \phi) + 2\sum_{k=1}^{N-1}\cos k(\theta - \theta_j + \phi)\right\} d\phi \\ &= \frac{2\pi}{N}\ln a - \sum_{k=1}^{N-1}\frac{1}{k}\cos k(\theta - \theta_j) + \frac{1}{2N}\cos N(\theta - \theta_j)\end{aligned} \tag{71}$$

by noting that:

$$\begin{aligned}\int_0^{2\pi} \ln\left|4\sin^2\frac{\phi}{2}\right| \cos k(\theta - \theta_j + \phi)\,d\phi &= Re(e^{ik(\theta-\theta_j)} I_k) \\ &= -\frac{2\pi}{k}\cos k(\theta - \theta_j):\end{aligned} \tag{72}$$

Therefore if operator $B = B_S + B_{NS}$, where B_S is singular and B_{NS} is non-singular, then:

$$(Bf)(\theta) = (B_{NS}f)(\theta) + \sum_{j=0}^{2N-1} w_j(\theta) f(\theta_j):$$

3.6 Numerical integration over an infinite range

When we numerically integrate operator C, we need to integrate across the real line $(-1; 1)$. This integral has no dependency on the integral over the pipe boundary so we can independently choose the optimal way to integrate over θ_1. The most obvious way is to use the trapezium rule but this produces

poor convergence rates of $O(h^2)$ where $h = R/N$ with R arbitrarily large.

As explained in *x*3.2, an improvement to this approach would be to use Gaussian quadrature, which for a smooth kernel would be extremely accurate for relatively few points (N 32) - Gauss-Hermite would probably give rapid convergence here. However, the kernel becomes singular as the load point approaches the line $y = Y$, which is a problem when we want to solve for all points in the domain D. Gauss-Hermite quadrature also performs best when the integrand decays exponentially as $jxj \; ! \; 1$ which may not be the case in this problem.

An alternative approach is to make a substitution in the integral to give us nite limits so we can then use Gauss-Legendre quadrature. For example, we can choose $x = \tan(\ )$. Thus the range for is $(\ \frac{}{2}; \frac{}{2})$. This substitution e ectively gives us a large x as x approaches 1 where we know the solution decays to 0, and a much smaller x near $x = 0$ where we need a much more granular discretisation. There are some limitations to using this quadrature which we have stated previously, but in the examples we have used this produces the best convergence.

The equation for operator C now becomes:

$$Cz(\mathbf{p}\ ) = \quad 2 \int_{\frac{}{2}}^{\frac{}{2}} G(\mathbf{p}\ ; \mathbf{q}(\ ))j_{y_q = Y}\, z(\ ) \sec^2 \quad d \ : \tag{73}$$

This kernel is not singular for $\mathbf{p} \; 2 \; _a$ if $Y > a$. However, we still have the problem of near singularity for those points $\mathbf{p} \; 2 \; D$ as $\mathbf{p}$ approaches $_1$. An improvement is achieved by splitting the integral into two domains $(-1 ; x_p)$ and $(x_p; 1\ )$, and using the substitutions $x = x_p \quad \tan$ on the rst domain, and use $x = x_p + \tan$ on the second domain. This ensures that the point of singularity (i.e. $x = x_p$) is the upper boundary on the rst integral and the lower boundary on the second integral.

We can then use Gauss-Legendre quadrature as described above on both integrals with grading if necessary. The operator C is then transformed to:

$$Cz(\mathbf{p}\ ) = \quad \frac{1}{2} \int_{0}^{\frac{}{2}} \ln \ \tan^2(\ ) + (Y \quad y_p)^2 \ [z(x_p + \tan\ ) + z(x_p \quad \tan\ )] \sec^2 \quad d \tag{74}$$

Given that we have a nite range, we generally use Gauss-Legendre integration with 64 points or with grading we use 8 points on 8 graded domains. This approach shows distinctly better convergence when $\mathbf{p}$ approaches the line $y = Y$ over other traditional approximations such as trapezium rule with $x = \tan$ substitution.

3.7 Error Analysis

We now examine the error for these composite rules to see what order of magnitude we should expect for a given discretisation. This will then give us some basis on which rule to choose for our numerical integration given other considerations such as speed and memory constraints.

3.7.1 Trapezium Rule

We expand the derivation given in Kress for clarity [11, p.198].

Theorem 6. *Let the remainder R(f) be de ned as:*

$$R(f) = \int_a^b f(x)dx \quad h\left[\frac{f(x_0)}{2} + f(x_1) + :::: + f(x_{N\ 1}) + \frac{f(x_N)}{2}\right] : \tag{75}$$

Then $jR(f)j \quad \frac{h^2}{12}(b \quad a)\ f^{00}{}_{1}$.

Proof. De ne $K(x)$ for each partition of the interval [a,b].

$$K(x) = \begin{cases} \frac{1}{2}(x \quad x_0)(x \quad x_1) & x_0 \quad x \quad x_1 \\ :::: & \\ \frac{1}{2}(x \quad x_{j\ 1})(x \quad x_j) & x_{j\ 1} \quad x \quad x_j \\ :::: & \\ \frac{1}{2}(x \quad x_{N\ 1})(x \quad x_N) & x_{N\ 1} \quad x \quad x_N \end{cases} \tag{76}$$

We integrate by parts twice to obtain:

$$\begin{aligned} \int_{x_{j\ 1}}^{x_j} K(x)f^{00}(x)dx &= \frac{y(y \quad h)}{2} f^{0}(y + x_{j\ 1}) \Big|_0^h - \int_0^h (y \quad \frac{h}{2}) f^{0}(y + x_{j\ 1}) \\ &= 0 \quad (y \quad \frac{h}{2}) f(y + x_{j\ 1}) \Big|_0^h + \int_0^h f(y + x_{j\ 1})dy \\ &= \frac{h}{2}[f(x_{j\ 1}) + f(x_j)] + \int_0^h f(y + x_{j\ 1})dy \\ &= \int_{x_{j\ 1}}^{x_j} f(x)dx \quad \frac{h}{2}[f(x_{j\ 1}) + f(x_j)] : \end{aligned} \tag{77}$$

Summing over $j = 1; : : : ; N$ we get:

$$\begin{aligned} jR(f)j &\sum_{j=1}^{N} \int_{x_{j\ 1}}^{x_j} K(x)f^{00}(x)\ dx \\ &\quad f^{00}{}_{1} \sum_{j=1}^{N} \int_0^h j\frac{y(y \quad h)}{2} jdy \\ &= f^{00}{}_{1} \sum_{j=1}^{N} \frac{hy^2}{4} \quad \frac{y^3}{6} \Big|_0^h \\ &= f^{00}{}_{1} \frac{Nh^3}{12} \\ &= \frac{h^2}{12}(b \quad a)\ f^{00}{}_{1} : \end{aligned} \tag{78}$$

□

3.7.2 Trapezium Rule on Periodic Functions

In the problem we are looking at, we know that our integrand is 2π-periodic around the pipe boundary. Therefore we can use a special feature of the trapezium rule which improves our accuracy from $O(h^2)$ considerably [10].

The most convenient way to analyse the periodicity is to look at the discrete Fourier transform of the integrand f.

$$f(x) = \frac{1}{2\pi} \sum_{m=-\infty}^{\infty} c_m e^{imx}$$

where

$$c_m = \int_0^{2\pi} f(x) e^{-imx} \, dx$$

trarily small, since standard Fourier analysis tells us that the coe cients c_m are of order $O(\frac{1}{m^{p+1}})$ for a p-times di erentiable function. However, for a function f whose derivatives are all periodic, there may exist values of N where the error is signi cant.

For example, $f(x) = \cos^5 x$, has a discrete Fourier transform:

$$f(x) = \frac{1}{2} \sum_{m=-5}^{5} c_m e^{imx}$$

where $c_{-5} = \frac{}{16}; c_{-3} = \frac{5}{16}; c_{-1} = \frac{5}{8}; c_m = 0$ otherwise. Since $c_0 = 0$ the exact value of the integral should be 0. From (80) we can see that if we use $N = 1; 3; 5$ we will get errors $2\ ; \frac{5}{8}; \frac{}{8}$ respectively and zero error for other values of N. Thus predicting a value for N which will give an arbitrarily small error for a general function f, is di cult to do analytically and will in all likelihood involve some trial and error.

Alternatively, by using repeated integration by parts on (80), we get the result that:

$$\int_0^{2} f(x$$

4 Numerical Examples for a buried pipe

4.1 Exterior Neumann problem on an unbounded domain

4.1.1 Analytic Solution

In order to test our methodology outlined above, and to examine the accuracy of our numerical implementation, it is usual to benchmark using a simple example where the anaytical result is known. Since we know with 100% con dence the true result we can therefore draw conclusions from our numerical approach.

The rst example we will look at is solving Laplace's equation with Neumann boundary conditions on an unbounded exterior domain, where the boundary is the rim of the pipe of unit radius. In physical terms, this means that the pipe is deep underground (we set Y = 100,000) and we set $a = 1; c = 0; g = 0$. In order to satisfy the compatability condition, from (14), we must ensure that $\int_a f = 0$. Choosing $f = \frac{x}{\sqrt{x^2 + y^2}}$ in Cartesian terms, satis es this condition and makes the problem solvable analytically. We have also stipulated earlier that $v \to 0$ as $|x|, |y| \to \infty$.
If we now transform this problem into polar coordinates (r, θ) then:

$$\begin{aligned} r^2 v_{rr} + r v_r + v &= 0 \\ \frac{\partial v}{\partial r}(a, \theta) &= \cos\theta \\ \lim_{r \to \infty} v(r, \theta) &= 0. \end{aligned} \tag{82}$$

Using separation of variables $v(r, \theta) = R(r)\Theta(\theta)$, we obtain:

$$\begin{aligned} \frac{r^2 R'' + r R'}{R} &= \\ \frac{\Theta''}{\Theta} &= \end{aligned} \tag{83}$$

where is a real constant.

Since v is 2π periodic, so is Θ, and therefore must be a positive constant to give a solution of the form $A\cos\sqrt{\ }\theta + B\sin\sqrt{\ }\theta$. Moreover to satisfy periodicity, = =

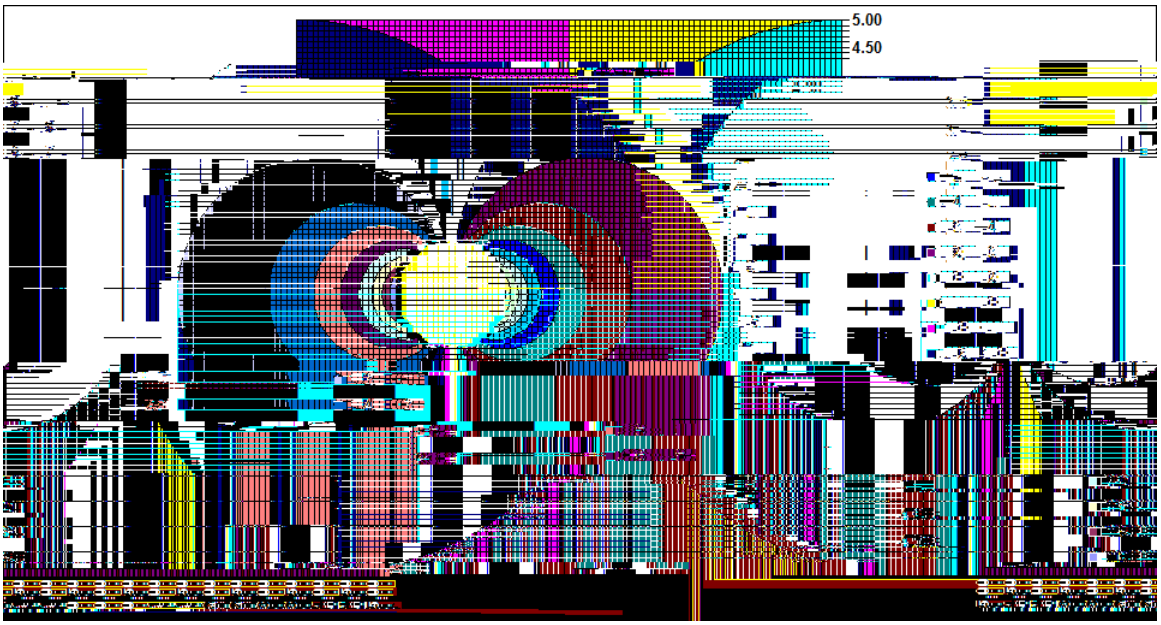

Figure 5: Analytic solution over a square subset of the domain D [-5,5] [-5,5]

4.1.2 Numerical Solution

We now need to compare this analytic solution to that obtained when we solve using the BIE (44).

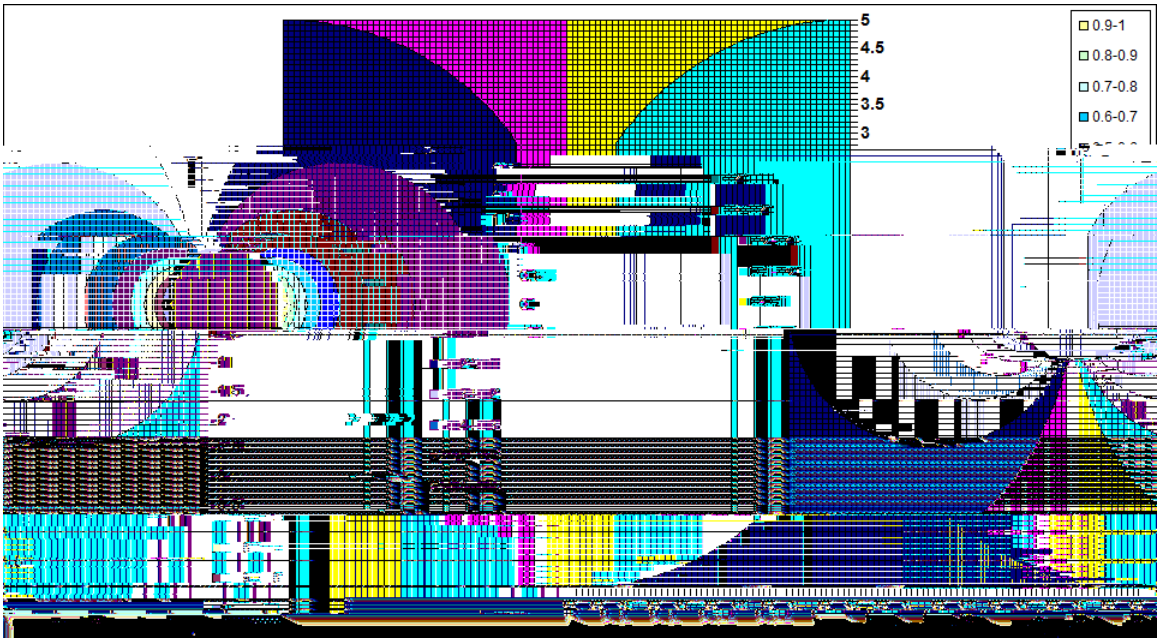

Figure 6: Numerical solution over a square subset of the domain D [-5,5] [-5,5]

We have used the Lagrange trigonometric basis functions as de ned in (57) for v and f and numerically

integrated using the composite trapezium rule. As demonstrated above, since the integrands are 2 - periodic, this should give us extremely fast convergence for relatively small M; in this example we are using $M = 64$. We notice that the analytic and numeric solutions in Figures 5 and 6 look very similar.

4.1.3 Global Error Observations

Although the two graphs at rst glance look very alike, there are some signi cant errors near the pipe boundary which the graph below highlights. This is to be expected since there is a discontinuity in the solution when p *2* $_a$. This is a feature of the Green's function only being integrated over a semi-circle to keep within the domain D, rather than over a full circle when the point is inside D.

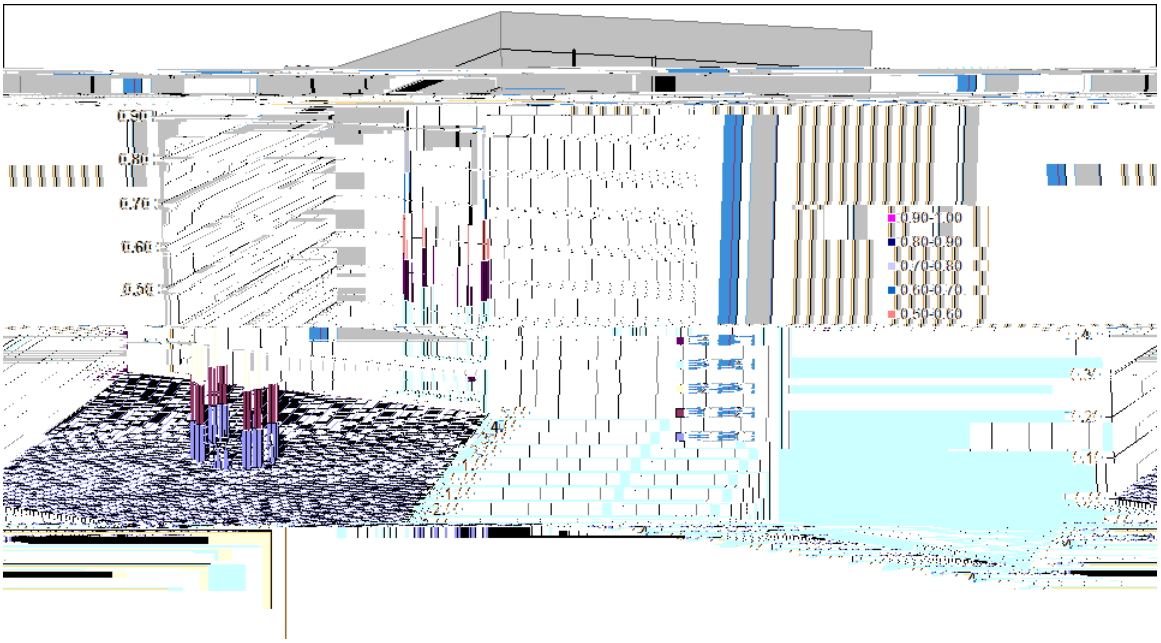

Figure 7: Graph of absolute errors - di erence between analytic and numerical solutions

There are several ways we can try to minimise this error:

Sample Points

Increase the number of sample points on the boundary $_a$. This is a sledgehammer approach since we only need to increase granularity when p is approaching the boundary. When p is su ciently far away a small number of sample points is perfectly adequate as the graph shows.

Collocation Points

Increase the number of collocation points used in the numerical integration when p is su ciently close to $_a$. This is possible because we have expressed the solution in terms of Lagrange trigonometric basis functions. These allow us to interpolate any value of *v* around the boundary $_a$ even though we have only explicitly calculated N values from the BIE. However, each basis function is usually expressed as a sum of $\frac{M}{2}$ trigonometric terms which6ofofire11 9.9626 Tf 145.49483 0 0 118.189 cm []0 d

each interpolation only requires M calculations.

From (57) using $M = 2N$,

$$
\begin{aligned}
{}^{N}_{j}(x) &= \frac{1}{2N}\left[1 + \cos N(x - x_j) + 2\sum_{n=1}^{N-1}\cos n(x - x_j)\right] \\
&= Re\left\{\frac{1}{2N}\left[1 + e^{iN(x-x_j)} + 2\sum_{n=1}^{N-1} e^{in(x-x_j)}\right]\right\} \\
&= Re\ \frac{1}{2N}\ 2\frac{(e^{iN(x-x_j)} - 1)}{(e^{i(x-x_j)} - 1)} + (e^{iN(x-x_j)}
\end{aligned}
$$

$\frac{2}{x}$ $(e^{iN(x\,x_j}$ j j18]TJ021342 Tf 9f 3.722 0. 1Td 5

We can therefore estimate v_{rr} at $r = a$ by using boundary data and estimating v with the three point approximation,

$$v \quad = \frac{v(\quad + \quad) + v(\quad \quad) \quad 2v(\ )}{2}$$

where can be arbitrarily small and the values of v

4.1.4 L2 norm error

When measuring the average global error of the numerical solution v_M on the boundary, we will use the L_2 norm on $v(\ _i)\quad v_{2N}(\ _i)$ for 10,000 points on $\ _a$. This should give us an indication of the speed of convergence of the solution as we increase N.

The formulation for the L2 error is:

$$E_{2N} = p\frac{1}{10000}\,kv(\ )\quad v_{2N}(\ )k_2$$

$$= p\frac{1}{10000}\,[v(\ _1)\quad v_{2N}(\ _1)]^2 + [v(\quad v_{2N}(\ )]^2 + \qquad + [v(\ _{10000}v_{2N}(\ )^2$$

4.2 Exterior Neumann problem on a semi-in nite domain

In example *x*4.1, as the pipe was deep underground, we ignored the boundary condition at ground level since this had negligible e ect on the solution. In this example we still want to compare our numerical results with the analytic solution, so we set $Y = 2$ and set the boundary values on the line $y = Y$ to be:

$$v = \frac{a^2 \cos\ (x; Y)}{r(x; Y)}:$$

We can easily re-express this in Cartesian terms so that:

$$\begin{aligned} v(x; Y) &= \frac{a^2 x}{(x^2 + Y^2)} \\ \frac{@v}{@y}_{y=Y} &= \frac{2a^2 xY}{(x^2 + Y^2)^2}: \end{aligned} \tag{91}$$

We do not expect discontinuous solutions on the boundary $y = Y$, since integrating both the Green's function at the load point and at the re ected point ensure there is no jump discontinuity when $p\ 2\ _1$. We should also note that this is a well-posed problem since the compatability condition is satis ed. In fact, g is an odd function so will always integrate to 0 over the real line.

This example will therefore test that our formulation for all operators A,B and C is correct and give con dence that we can solve any exterior problem with good accuracy (away from the vicinity of the pipe boundary).

4.2.1 Numerical Solution

The following graph is a surface plot of the solution v in the box [-2,2]*23 (of) . e t inc e*

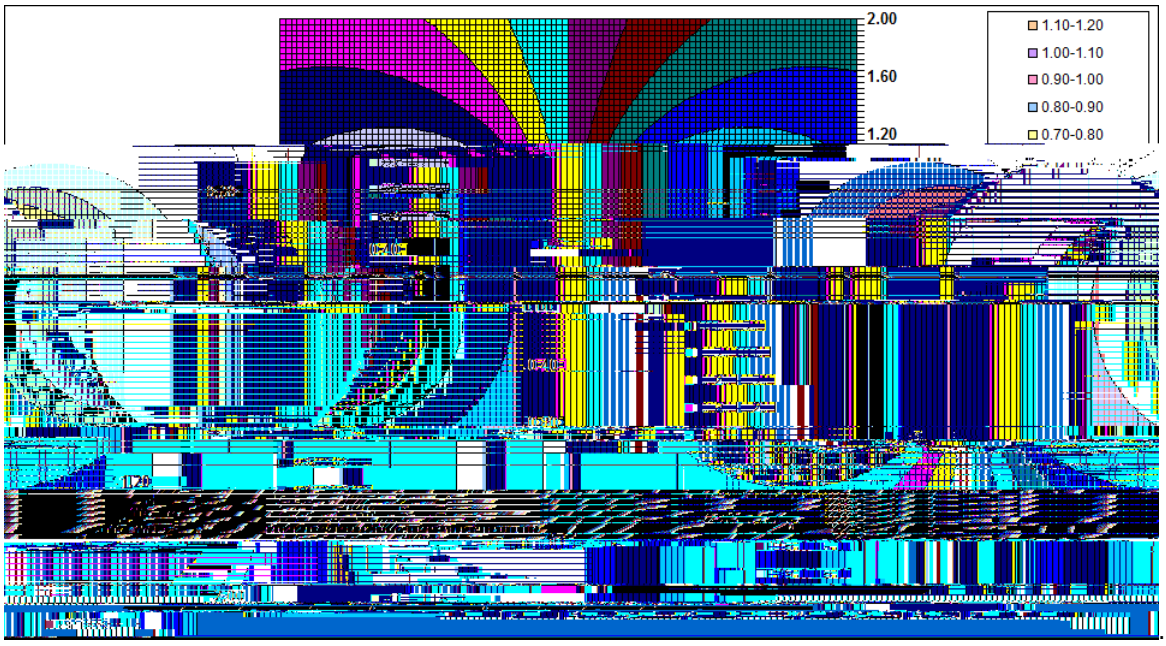

Figure 9: Graph of numerical solution with Y=2.0

4.2.2 Global Error Observations

Next we plot the global error between the analytic solution from the example *x*4.1 and the numerical solution. The rst graph shows errors without re nement near the boundary, the second includes the re nement. As with the previous example, a considerable error reduction is observed.

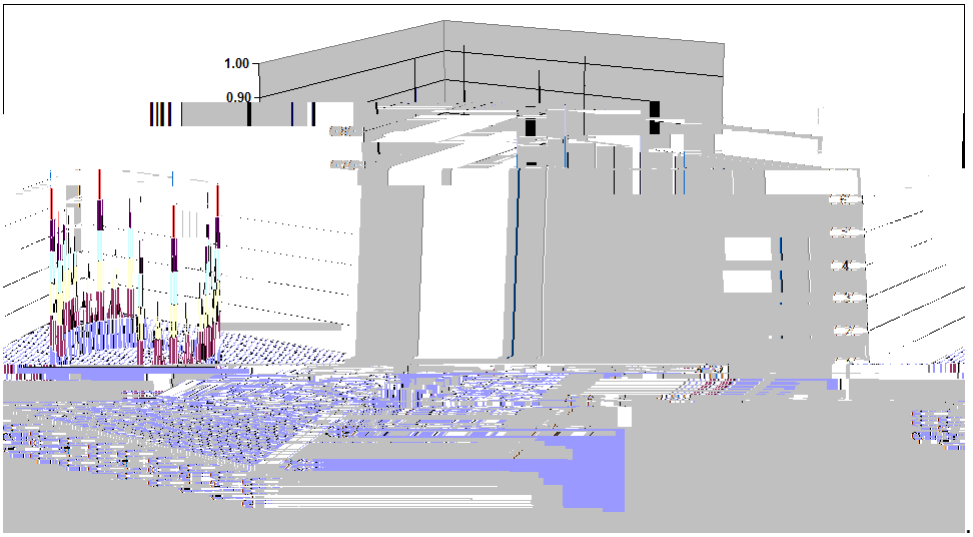

Figure 10: Absolute errors between analytic and numerical solution with Y=2.0

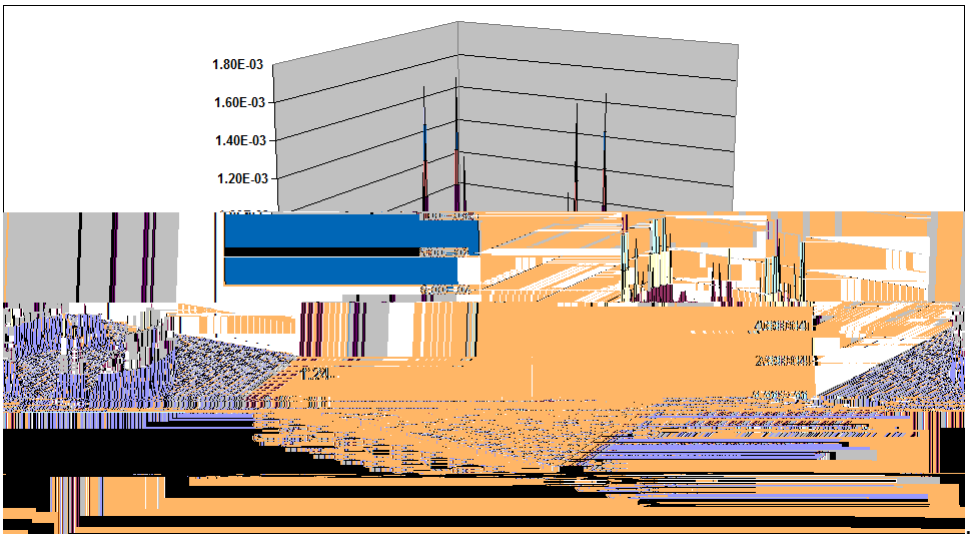

Figure 11: Absolute errors between analytic and re ned numerical solution with Y=2.0

4.2.3 L2 norm error

Table 4 shows the average global error for values of v on $_a$ using di erent numbers of sample points. Again this shows better than exponential convergence in the solution to 32 points at which point numerical precision dominates the error term.

M	L_2 error
4	8.829 x 10 ^{3}
8	1.172 x 10 ^{4}
16	1.420 x 10 ^{8}
32	9.316 x 10 ^{10}
64	1.310 x 10 ^{9}
128	1.823 x 10 ^{9}

Table 4: L2 error for v on the boundary $_a$

Table 5 shows the average global error for values of v in the domain D. A square grid of points is generated in this case using 100 100 in the $(x;y)$-region [-2,2] [-2,2] and the average L_2 norm is again calculated on these 10,000 points using di erent values of N. The outlying error values on the pipe boundary are excluded in order to ascertain the rate of convergence in the region where the solution is well-behaved. In addition, we have also excluded the points that lie on the line $y = Y$ since these values are subject to small errors caused by the integration over $_1$ where there is a singularity in G. These errors tend to dominate the L2 norm error and hence cloud any trend in the convergence rate elsewhere in the domain.

We can see that rate of convergence is nearly exponential up to $M = 64$ but at which point, errors

in the integration across $_1$ dominate since this is dependent on how many sample points we use on the top boundary and is independent of M.

M	L_2 error
4	8.433 x 10 ^{2}
8	1.375 x 10 ^{2}
16	1.074 x 10 ^{3}
32	1.407 x 10 ^{5}
64	1.949 x 10 ^{6}
128	1.949 x 10 ^{6}

Table 5: L2 errors for a grid of values v in D

4.3 Exterior Neumann problem on semi-in nite region with non-zero c

In this example, we introduce a non-zero c term which has an interesting e ect on the solution v near the pipe boundary. As described in $x1$, $u \to cy + T_0$ far away from the pipe. As temperature increases for large negative y; c must have a negative value. The variable v is independent of c, but it does a ect the boundary condition $\tilde{f} = f + c\sin\theta$. g is also independent of c, since $\frac{\partial u}{\partial y}$ and hence $g \to c$ as $|x| \to 1$.

For this example, we are considering $f = \cos\theta$. (A trigonometric condition is sensible since it has to be 2π-periodic). Therefore in this case:

$$\begin{aligned}\tilde{f} &= f + c\sin\theta \\ &= \sqrt{1+c^2}\left(\frac{1}{\sqrt{1+c^2}}\cos\theta + c\frac{1}{\sqrt{1+c^2}}\sin\theta\right) \\ &= \sqrt{1+c^2}\cos(\theta + \cos^{-1}\frac{1}{\sqrt{1+c^2}}).\end{aligned} \tag{92}$$

Hence the normal derivative has undergone a rotation of $\cos^{-1}\frac{1}{\sqrt{1+c^2}}$, and has been scaled up by $\sqrt{1+c^2}$.

4.3.1 Numerical Solutions

We illustrate this rotation and scaling in Figures 12{14 and also demonstrate convergence for a di erent number of sample points, M. We have used the same parameters as example $x4.2$, except that $c < 0$ and the boundary condition $g = xe^{-x^2}$. Again, this function is odd and therefore integrates to 0 over the real line.

Firstly, we show a plot using $c = -0.5$ and $M = 16$. For this number of sample points, we can observe a lack of convergence particularly around the pipe boundary. There is already a discernible rotation of the solution compared to example $x4.2$ at this point.

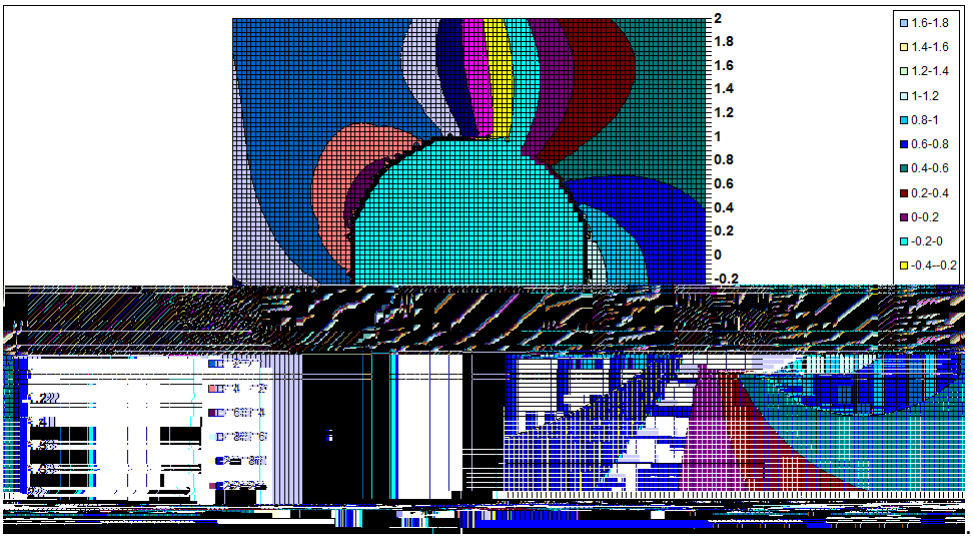

Figure 12: Graph of numerical solution - $Y = 2{:}0; c = \ 0{:}5; M = 16$

Next, we show the solution using $M = 64$. Here convergence has already taken place away from the pipe boundary and we can start to see that the solution has a similar pattern to example $x4.2$.

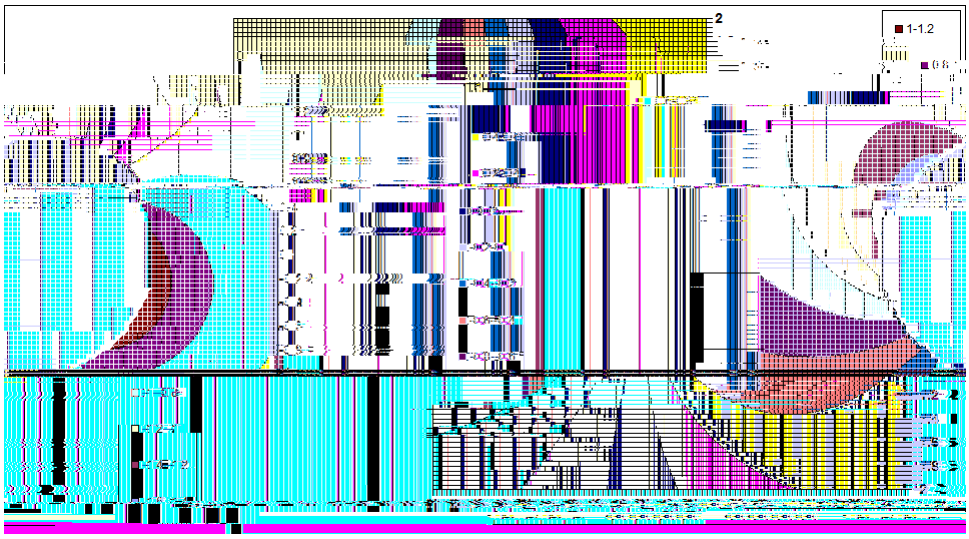

Figure 13: Graph of numerical solution - $Y = 2{:}0; c = \ 0{:}5; M = 64$

In Figure14, we are using $M = 256$. Given that convergence is established we will use this to be our \true" solution. Here we can see clearly that the solution, particularly around the pipe boundary, has been rotated by approximately $\frac{}{6}$ compared to the solution in example $x4.2$. The magnitude of the solution near the boundary is also larger - we would intuitively expect this since the solution still has to decay to zero for large values of $x; y$ but we start with a larger normal derivative on the boundary.

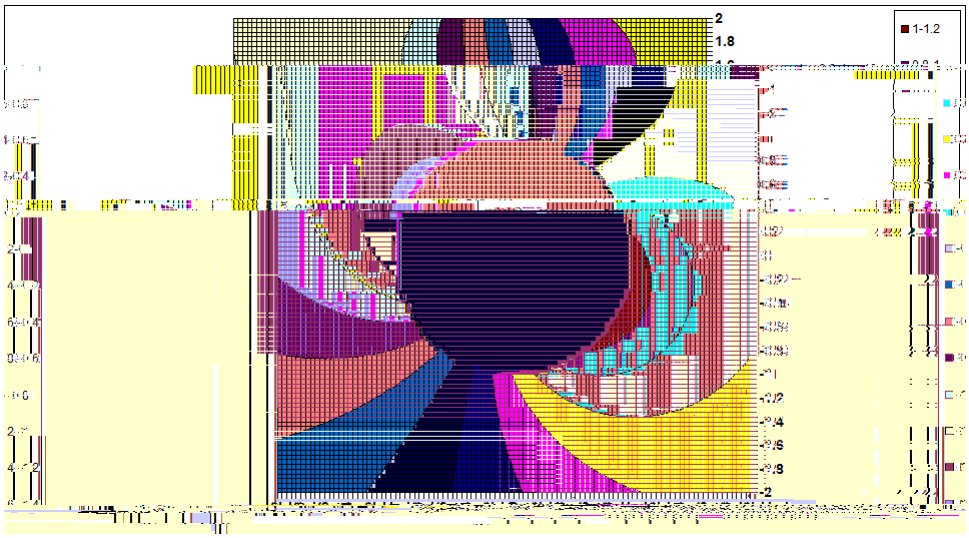

Figure 14: Graph of true numerical solution - $Y = 2{:}0; c = \ 0{:}5; M = 256$

Finally, we illustrate in Figure 15 the feature of rotation for a di erent value $c = \ 1$. Here we would expect a rotation of $\frac{}{4}$ and a scaling factor of $\overline{p\ 2}$ on the normal derivative versus the solution in example 4.2.

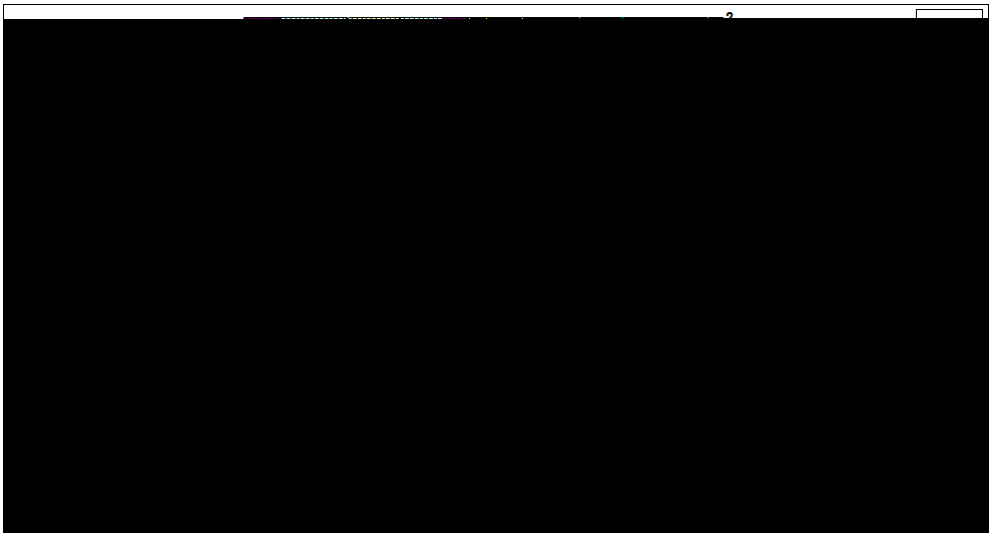

Figure 15: Graph of \true" numerical solution - $Y = 2{:}0; c = \ 1{:}0; M = 256$

Even though we have no analytic solution to compare to, we can still sense check some of the results. Clearly we can laboriously check that $r^2 v = 0$ by using the ve point formula that we used for Finite Di erences Method in $x1$. Additionally we can check that the numerical solution satis es the boundary conditions. Using the last example, we can evaluate $\frac{@v}{@n}; \frac{@^2 v}{@n^2}; \frac{@^3 v}{@n^3}$ using the nearest ve points to the boundary $y = Y$. Using Taylor's theorem, we can then get a numerical approximation for $\frac{@v}{@n}$ on the

boundary and compare it to the value given by the boundary condition. For the last example, the largest discrepancy using such a method was 2.0042 10 ^{4}. This gives us con dence that the model is converging to the correct values.

4.3.2 Global Error Observations

Figure 16 shows us the error between the two runs with 64 and 256 sample points. Again it clearly demonstrates convergence away from the pipe boundary and implies that relatively few sample points are needed for a convergent solution for a sparse grid of points in the domain, whilst if the focus is on accuracy around the pipe boundary then we need a larger number of sample points.

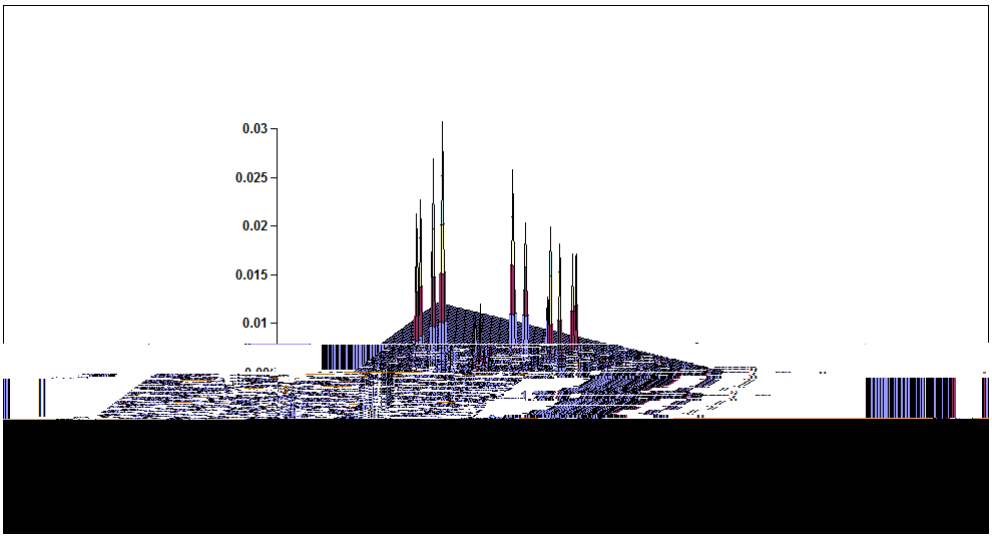

Figure 16: Absolute error - di erence between numerical solutions with 64 and 256 sample points

4.3.3 L2 norm error

Table 6 shows the average global error for values of v on the boundary $_a$ using di erent numbers of sample points. Again this shows exponential convergence in the solution to 32 points at which point numerical precision dominates the error term.

M	L_2 error
4	5.852 x 10 ^{2}
8	4.793 x 10 ^{3}
16	2.223 x 10 ^{5}
32	2.716 x 10 ^{9}
64	2.630 x 10 ^{9}
128	2.318 x 10 ^{9}

Table 6: L2 error of v on boundary $_a$

101 101 grid of solutions. The reason for including $Y = 1{:}04$ as one of our simulations is that solutions on $y = 1{:}00$ give us the closest comparison (one grid spacing di erence) to our solution for $Y = 1{:}00$ without the solution being singular on that line.

The results of the L2 errors are shown in Table 8:

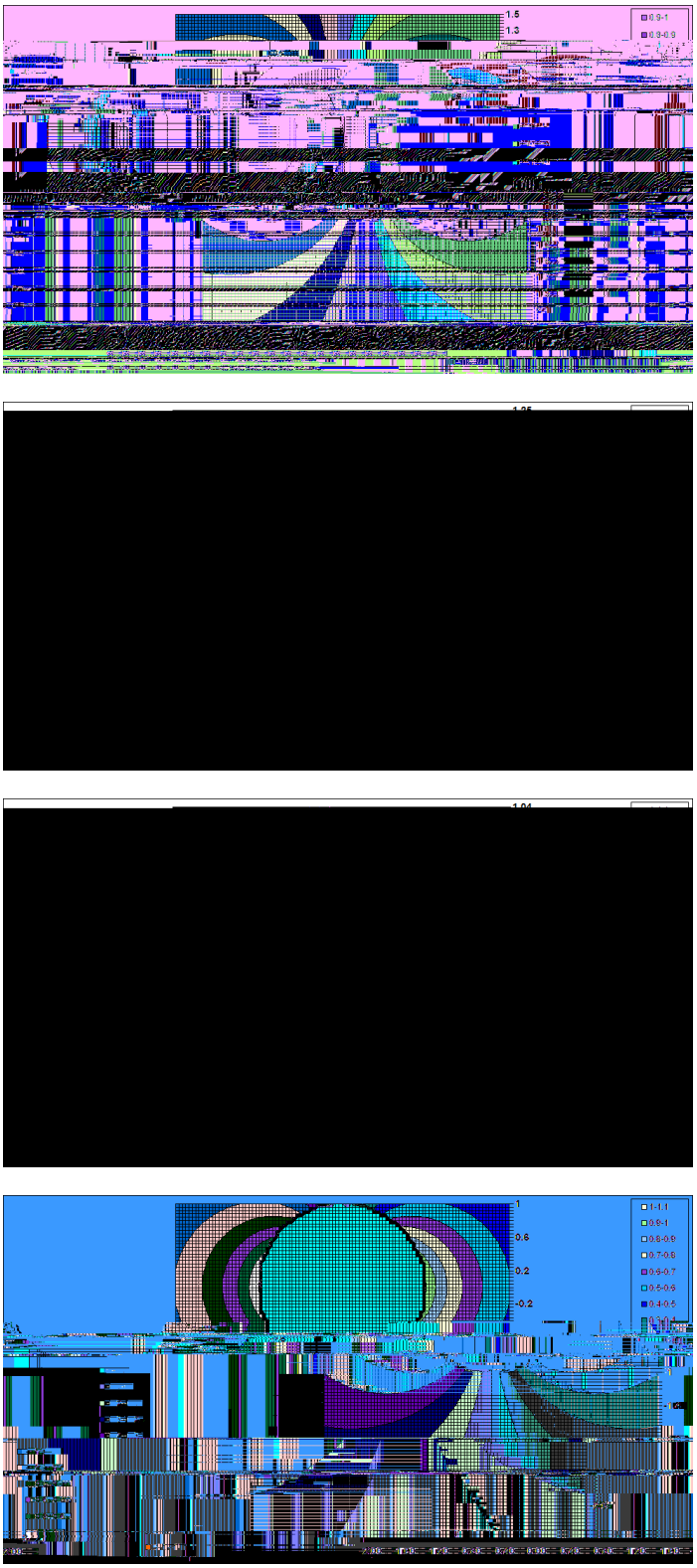

Figure 17: Evolution of numerical solution for $Y = 1.5; 1.25; 1.04; 1.0$

5 Partially Buried Pipe

In this section, we now look to reformulate our equations to deal with the situation where the pipe is only partially submerged underground. Firstly, we will need to rede ne our domains and boundaries and then also make sure that we can reapply Green's Second Identity on these new domains. Once this has been established, we will then revisit our previous examples to see what e ect the emergence of the pipe has on the solution in the domain.

5.1 Background

For the pipe to be only partially submerged underground, the condition $a < Y < a$ must hold. If $Y \quad a$, then the pipe is fully submerged and we can use our previous method. If $Y \quad a$, then the pipe is wholly above ground, and the problem reduces to one over a semi-in nite region where the pipe has no relation to the problem.

In terms of our de nitions, the main di erences are:

D_a is the interior of the circle centred at the origin with radius a. This bottom part of this region is underground, the top part above ground.

$_a$ is the circular arc that connects the two points of the circle D_a that intersect with the line $y = Y$. These two points are $\mathbf{p_1}; \mathbf{p_2}$.

$\mathbf{p_1} = (\ ^p\overline{a^2 \quad Y^2}; Y)$ and $\mathbf{p_2} = (+^p\overline{a^2 \quad Y^2}; Y)$.

$_1$ is now de ned on the line $y = Y$ but is split into two parts. The rst part runs from $(\ 1; Y)$ to $\mathbf{p_1}$, the second runs from $\mathbf{p_2}$ to $(+1; Y)$.

Our domain D, contains all points $\mathbf{p}$ where $y < Y$ and $\mathbf{p} \in D_a$.

These de nitions are illustrated in Figure 18.

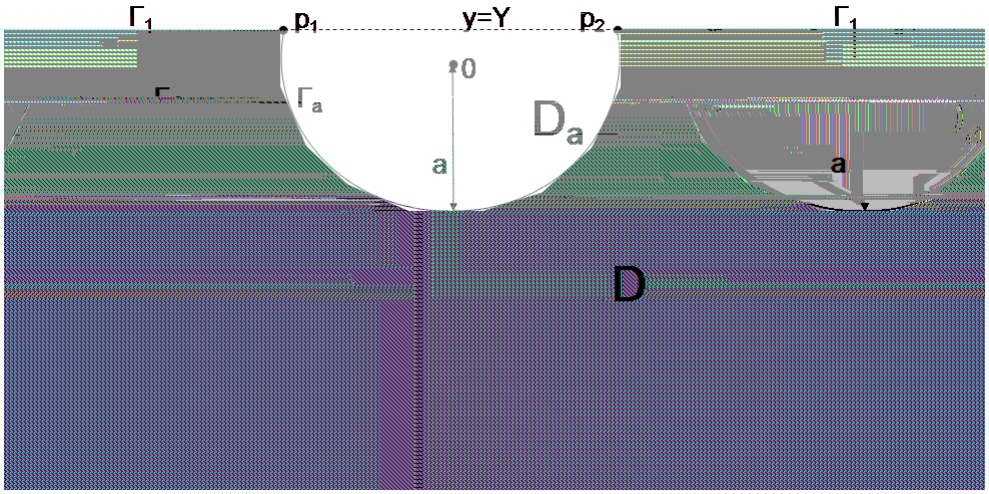

Figure 18: Layout for the partially buried pipe

5.2 Formulating the BIE

For the existence of a convergent solution we still need to stipulate that:

$v \to 0$ as $x \to \infty$.

$\frac{\partial v}{\partial n}$ must be $O(x^{-1-\alpha})$ for some $\alpha > 0$.

The compatability condition (14) must still hold for $\tilde{f}$ and g.

We are still solving for v over Γ_a, and using this boundary solution to solve for all points in the domain D.

There immediately appears to be a problem in defining the normal derivative $\frac{\partial v}{\partial n}$ at points $\mathbf{p_1}$ and $\mathbf{p_2}$, since at this intersection point the boundary has a discontinuous derivative. Given that there is also a discontinuity in the solution at the pipe boundary we may have to consider how we discretise the problem as we approach both Γ_a and Γ_1.

Using the new definitions, we can apply Green's Identity as before on the domain D.

For $\mathbf{p} \in D$:

$$v(\mathbf{p}) = \int_{\Gamma_a} \left(\frac{\partial G}{\partial n_q}(\mathbf{p};\mathbf{q}) v(\mathbf{q}) - G(\mathbf{p};\mathbf{q}) \tilde{f}(\mathbf{q}) \right) ds_q - \int_{\Gamma_1} G(\mathbf{p};\mathbf{q}) g(\mathbf{q}) ds_q. \tag{93}$$

For $\mathbf{p} \in \Gamma_a$:

$$\frac{v(\mathbf{p})}{2} - \int_{\Gamma_a} \frac{\partial G}{\partial n_q}(\mathbf{p};\mathbf{q}) v(\mathbf{q}) = - \int_{\Gamma_a} G(\mathbf{p};\mathbf{q}) \tilde{f}(\mathbf{q}) ds_q - \int_{\Gamma_1} G(\mathbf{p};\mathbf{q}) g(\mathbf{q}) ds_q. \tag{94}$$

Thus to solve (94), we must integrate round Γ_a from points $\mathbf{p_1}$ to $\mathbf{p_2}$, and similarly for Γ_1 we must use quadrature along the line $y = Y$, omitting the interval $[-\sqrt{a^2 - Y^2}; +\sqrt{a^2 - Y^2}]$.

5.2.1 Numerical integration using mollifiers

Turning our attention initially to the right hand side (RHS) of (94), numerically this is equivalent to integrating around the whole pipe boundary and along the whole real line, and setting the functions $\tilde{f}; g$ to zero where the range of integration needs to be omitted. The only extra stipulation for the composite trapezium rule to work is that the function $\tilde{f} \in C^1$, so that the discontinuities across points $\mathbf{p_1}$ and $\mathbf{p_2}$ are smoothed out. Since we are using Gaussian quadrature to integrate across the real line, this condition need not apply to g.

Let the modified function be f, so that $f(\ ) = \tilde{f}(\ )(\ )$. We choose $(\ )$ in such a way that:

$f = \tilde{f}$ for all collocation points on the pipe boundary where $y_q \leq Y$

$f = 0$ for all collocation points where $y_q > Y$.

We also need to ensure that $2 C^1$, and that all derivatives of f and $\tilde{f}$ are equal at points $\mathbf{p_1}; \mathbf{p_2}$. This is equivalent to stipulating that all derivatives of are zero at points $\mathbf{p_1}; \mathbf{p_2}$.

Tests show that this approximation does give reasonable accuracy for $N = 64$. However as N is increased the approximation oscillates around the convergent value. This is probably because the Fourier series required to t the function requires many terms given the discontinuity, and as we observed before N must be greater than the order of the Fourier series to obtain super-algebraic convergence.

5.2.2 Numerical integration using grading

Operators A,B

Another more obvious approach is to integrate around the circle from $_1$ to $_2$ using Gaussian quadrature with grading. When we were integrating round a full circle we were able to isolate the singularity using the properties of the Lagrangian basis functions. However, we now know that for p 2 $_a$ there will be a singularity in the integrand.

Supposing this singularity occurs when = , then we should perform Gaussian quadrature with grading from $_1$ to and also from to $_2$. Using 8 points for each graded domain should ensure better convergence than for 64 points with no grading.

Operator C

When integrating operator C, we may also need to re ne our methodology since if we simply make $g(\tilde{x}) = 0$ in the range $[x_1; x_2] = [a\cos\ _1; a\cos\ _2]$, then $\frac{@g}{@x}$ x],

eral regions resulting in the following integ

$$\int dx_q + \int_{|x_p|}^{x_2} G(x_q) g(x_q) d$$

$$\int dx_q + \int_{|x_p|}^{1} G($$

$$+ G($$

(98)

e can use grading with 8 points on 8 domains obtain optimal accuracy.

5.3 pipe

5.3 d pipe

We ed previously with an example. In order to compare against an a half buried pipe where $Y = 0$. The boundary conditions are:

$$f(\ ) = \cos$$

$$g(x) = 0.$$

This on $v = \frac{\cos}{r}$.

The r Gaussian quadrature with grading does take longer to calculate than f ill look at a coarser grid of 41 41 solutions over the region [-2,2] [- we will show in Table 9 the L2 error (the di erence between the num r all points, and the time taken to calculate solutions for both methods

	L_2 error	Calculation time (secs)

solved for a grid 41 41 points in the region [-1,1] [Y-2,Y]. For each value of $Y = 0{:}50; 0{:}00; 0{:}50; 0{:}90$, we run the simulation using $M = 64$ with graded quadrature. For the case Y

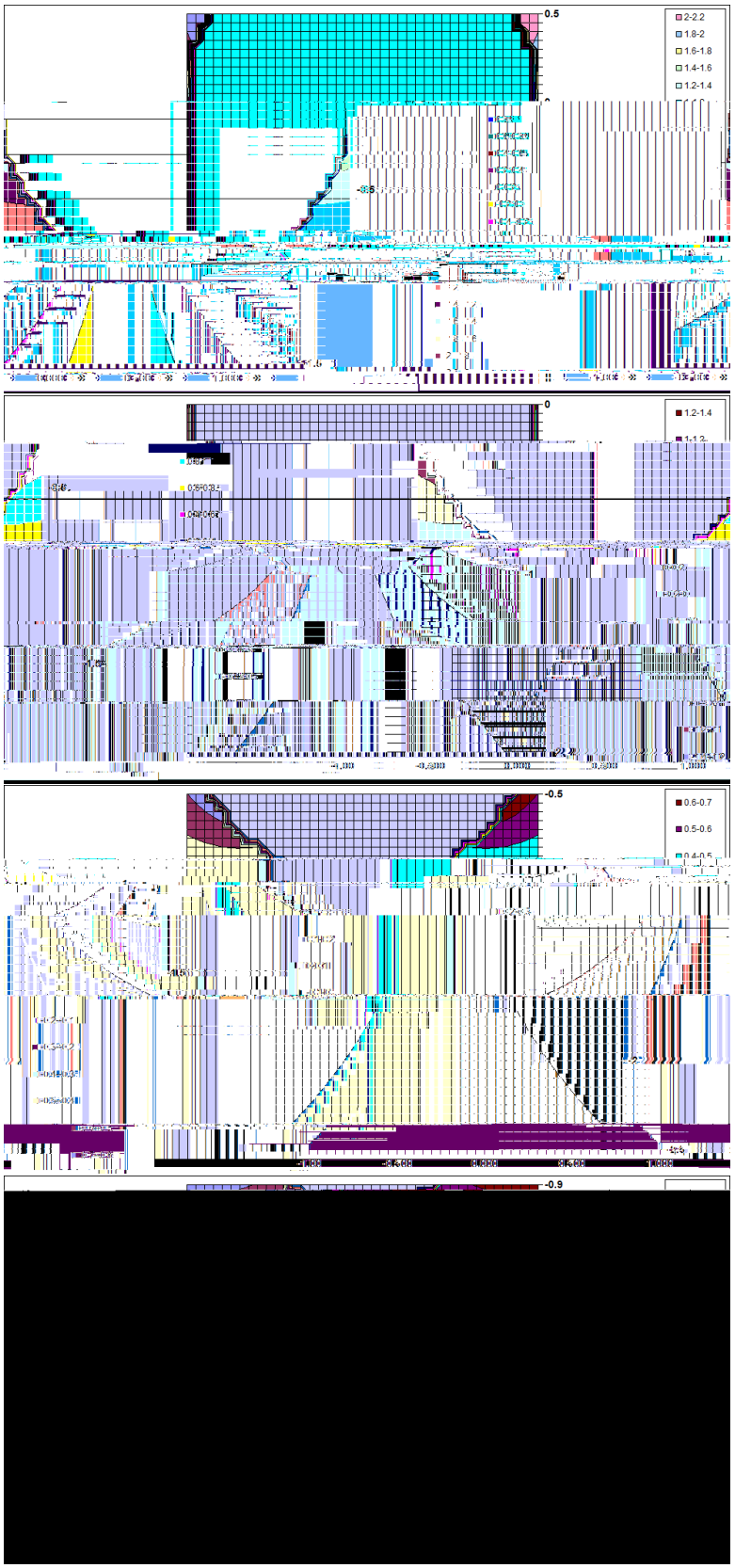

Figure 20: Evolution of solution as Y goes from +0.5 to -0.9

References

[1] M. Abramowitz and I. Stegun: Handbook of Mathematical Functions, Dover (2006)

[2] K. Atkinson: Numerical Solutions of Integral Equations of the Second Kind, Cambridge University Press (1997)

[3] H. Bau: Cognitive Heat Losses from pipe buried in semi-in nite porous medium, International Journal of Heat and Mass Transfer, Vol 27, Issue 11, pp 2047-2056 (1984)

[4] H. Bau and S. Sadhal: Heat Losses from Fluid Flowing in a Buried Pipe, International Journal of Heat and Mass Transfer, Vol 25, Issue 11, pp 1621-1629 (1982)

[5] W. Briggs and Van Emden Henson: The DFT - an owner's manual for the discrete Fourier Transform,SIAM (1995)

[6] O. Bruno, C. Geuzaine, J. Monro, F. Reitich: Prescribed error tolerances within xed computational times for scattering problems of arbitrarily high frequency, The Royal Society, pp 629-645 (1984)

[7] M. Chung, P. Jung and R. Rangel: Semi-analytical solution for heat transfer from a buried pipe with convection on the exposed surface, International Journal of Heat and Mass Transfer, Vol 42, pp 3771-3786 (1999)

[8] A. Dayan, A. Merbaum and I. Segal: Temporary Distributions around Buried Pipe Networks, International Journal of Heat and Mass Transfer, Vol 27, Issue 3, pp 409-417 (1984)

[9] P. DuChateau, D. Zachmann: Schaum's Outline of Partial Di erential Equations (1986)

[10] S. Johnson: Notes on the convergence of Trapezoidal Rule Quadrature, http://math.mit.edu/stevenj/trapezoidal.pdf (2010)

[11] R. Kress: Linear Integral Equations - Second Edition, Springer-Verlag (1999)

[12] S. Langdon: Pers. Comm. (2010)

[13] C. Ovuworie: Partially Buried Pipe Heat Transfer Presentation (2008)

[14] C. Ovuworie: Steady-State Heat Transfer Models For Fully And Partially Buried Pipelines, Society of Petroleum Engineers (SPE) paper 131137-MS, 2010 (doi 10.2118/131137-MS)

[15] A. Sadegh, L. Jiji and S. Weinbaum: Boundary integral equation technique with application to freezing around a buried pipe, International Journal of Heat and Mass Transfer, Vol 30, Issue 2, pp 223-232 (1987)

[16] F. Scheid: Schaum's Outline of Theory and Problems of Numerical Analysis, Second Edition (1989)

[17] I. Sloan: Error Analysis of boundary integral methods, Acta Numerica, pp 287-339 (1991)

[18] Web page: http://en.wikipedia.org/wiki/Bipolar_coordinates

[19] Web page: http://en.wikipedia.org/wiki/TauTona_Mine

[20] Web page: http://en.wikipedia.org/wiki/Two-center_bipolar_coordinates

[21] Web page: http://www4.ncsu.edu/ rsmith/MA573_F09/Heat_Equation.pdf